2011 11th IEEE International Conference on Nanotechnology
Portland Marriott
August 15-18, 2011, Portland, Oregon, USA

Electrical characteristics of carbon nanofibers in air and vacuum

Nobuhiko Kanzaki[1], Patrick Wilhite[1], Shusaku Maeda[2], Toshishige Yamada[1], and Cary Y. Yang[1]
[1]Center for Nanostructures, Santa Clara University, Santa Clara, CA 95053, USA
[2]Hitachi High-Technologies Corporation, Ibaraki, Japan
Email: NKanzaki@scu.edu

Abstract − We present a study on the effect of ambient gases on the electrical properties of carbon nanofibers (CNFs). The resistances of a CNF placed horizontally on a substrate in air and in vacuum are compared. CNFs in air show much lower current capacities compared to those in vacuum. Joule heat produced by constant current stressing results in desorption of gas molecules responsible for carrier trapping, leading to a lower resistance. In air, the resistance returns to its room-temperature value after cooling down. However, in vacuum, where most desorbed gaseous species are evacuated before any significant re-adsorption can occur, the room-temperature resistance continues to decrease with increasing stress current. A model is proposed to describe these observations, and is used to estimate the number of adsorbed molecules on the CNF.

Index Terms – carbon nanofiber, resistance, molecular sensor

I. Introduction

Nanoscale carbon structures, such as carbon nanotube (CNT) [1-3] and carbon nanofiber (CNF) [4-6] are promising as potential next-generation interconnect materials due to their much higher current capacities than that of copper (Cu) [7,8]. In addition, CNF is a possible candidate for other nanoelectronics applications such as thermal interface materials and chemical sensors, because of their excellent thermal and electrical properties and low growth temperature [9,10]. Thus an in-depth understanding of the CNF electrothermal characteristics is necessary in evaluating its potential for these applications. In this paper, we report the resistance behavior of CNFs in vacuum, and compare with its counterpart under ambient conditions. Our results suggest that adsorption/desorption of gaseous molecules in atmosphere is the dominant mechanism underlying the observed differences in electrical characteristics.

II. Fubrication and Measurement

CNFs were grown using plasma-enhanced chemical vapor deposition (PECVD), with acetylene (C_2H_2) as the carbon source, ammonia (NH_3) as a reducing agent, and nickel (Ni) as catalyst [10]. After growth, the CNFs were suspended in isopropyl alcohol, and drop-casted between a pair of patterned gold (Au) electrodes on a SiO_2 substrate. Tungsten (W) was then deposited onto the CNF-Au contact using electron-beam-induced deposition (EBID) [11] to reduce the contact resistance. In this technique, the source gas is delivered via a specially designed gas injection system (GIS) and guided by the focused electron beam to yield deposition on a selected target at a low energy.

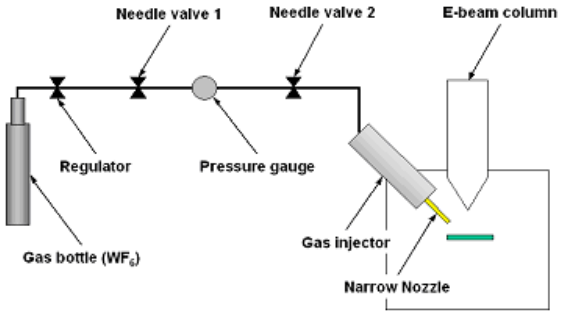

Fig. 1 Schematic of electron-beam-induced deposition apparatus including a gas injection system (GIS).

Figure 1 shows a schematic of the GIS, which is installed in the chamber of a variable-pressure scanning electron microscope (VP-SEM). The source gas for tungsten is WF_6. For this study, the working distance inside the SEM chamber is set to 12.5 mm, and the distance between the device surface and the nozzle tip is within 0.1 mm. The electron beam acceleration voltage is 30 kV with a beam current of 150 μA, resulting in substrate currents of ~30 pA. The target area is exposed to the e-beam for 30 minutes.

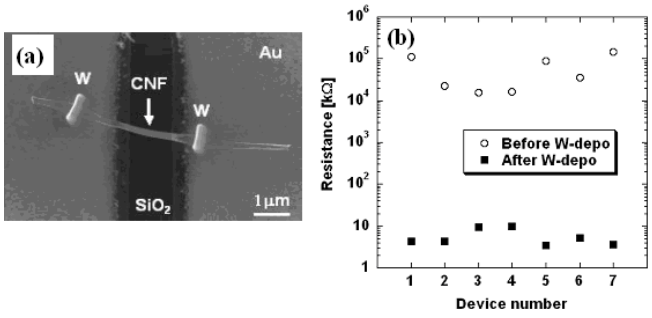

Fig. 2 (a) SEM image of CNF test device with W-deposited contacts. (b) Resistances of seven CNF test devices before and after W deposition.

Figure 2(a) shows the SEM image of a CNF with W-CNF-Au electrode contacts formed by e-beam deposition of W. The size of the W spot is in the 300-500 nm range. The measured resistances of seven devices before and after W deposition are shown in Fig. 2(b) and they decrease from well above MΩ to a few kΩ as a result of the deposited W contacts.

A series of progressively increasing constant currents are applied to each fabricated device. Between successive current stress cycles, when the device is cooled down to room temperature, low-voltage sweeps are performed to determine the resistance.

Samples measured under atmospheric conditions are tested using a wafer probe station which utilizes micromanipulators coupled to Kelvin probes. These probes rest on the Au pads of the device while current-voltage (*I-V*) measurements are performed with a semiconductor parameter analyzer. In vacuum, we use a similar configuration consisting of nanomanipulators with W probe-tips inside the chamber of a high-resolution SEM, with base pressure of about 1 x 10^{-4} Pa.

III. Results and Discussion

In ambient, the resistance measured after each stress cycle (at room temperature) is virtually unchanged, as shown in Fig. 3(a). In vacuum, however, the results after each stress cycle show a significant decrease in device resistance, as shown in Fig. 3(b). We attribute this observed behavior to carrier detrapping due to Joule heating, and re-trapping during the subsequent cooling.

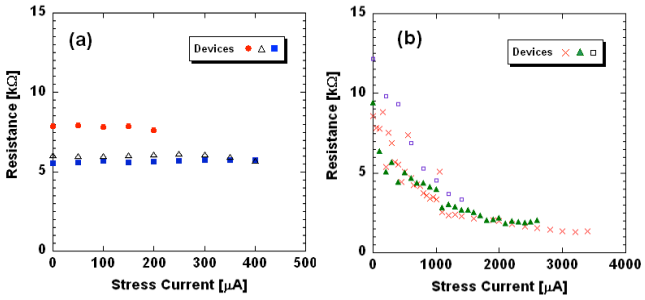

Fig. 3 Resistance of CNF in ambient (a), and in vacuum (b).

As we previously reported [12], the results in ambient suggest that carriers are trapped by defects along the conductive graphitic layers of the CNF at room temperature. In addition, some gaseous species adsorbed on the CNF can also serve as carrier traps, similar to other carbon nanostructures [13-16]. The trapped carriers are detrapped as a result of thermal activation by Joule heating when its temperature is increased due to current stressing. In atmosphere, these detrapped carriers are trapped again after the device returns to room temperature. Thus the measured resistance after each stress cycle remains constant until device breakdown.

However, when desorbed in vacuum through Joule heating, a significant amount of the gaseous species are evacuated, preventing re-adsorption onto the CNF and resulting in a continuous decrease in resistance as stress current increases. Furthermore, breakdown currents (as well as the corresponding current densities) for CNFs in vacuum are much higher than those in ambient (see Fig. 3). This is attributed to the much lower concentrations of oxidizing species such as oxygen and water molecules in vacuum, which have been shown to lead to carbon nanotube failure [13].

Figure 4 shows the SEM images of a CNF test device in vacuum subject to successive current stressing until breakdown. The images are taken after each stress cycle, as shown in Figs. 4(b) to 4(f). In this sequence, discernable changes occur on the outer layers of the CNF after 1100 μA. Significant CNF structure modification is observed after 2500 μA, although the resistance continued decreasing until breakdown at 2700 μA. The diameter of the CNF is 228 nm, yielding a breakdown current density of 6.6 x 10^6 A/cm^2.

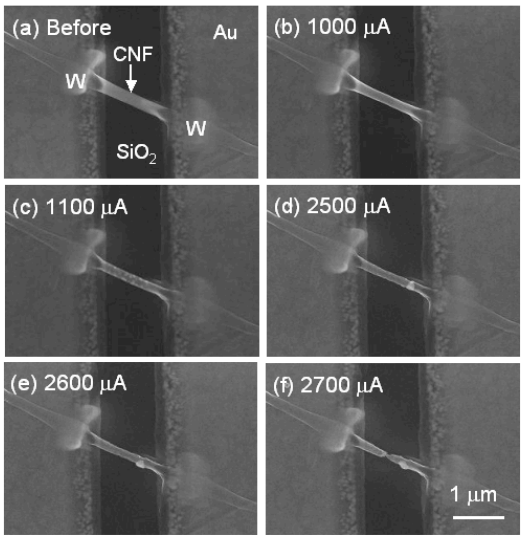

Fig. 4 SEM images of CNF test device before and after each stress cycle in vacuum: (a) before stress cycle, (b) after 1000 μA, (c) after 1100 μA, (d) after 2500 μA, (e) after 2600 μA, and (f) after 2700 μA when breakdown occurs.

We suggest that the difference in CNF resistance behavior between ambient and vacuum is caused by presence of gas molecules in air, in particular, oxygen and water vapor. Figs. 5(a) and 5(b) illustrate a model for gas molecule adsorption/desorption in ambient and in vacuum. In ambient, current flow is impeded by carrier trapping by the adsorbed molecules. These molecules are subsequently desorbed by Joule heating when stress current is applied to the CNF. However, these desorbed molecules are re-absorbed after the end of each stress cycle (when cooling occurs), and can again trap carriers. In vacuum, on the other hand, once the molecules are desorbed by Joule heating, they are evacuated. Since the amount of gas molecules remaining in the SEM chamber is roughly nine orders of magnitude less than in ambient, the probability of re-adsorption is significantly diminished. Thus the CNF

resistance after each stress cycle continues to decrease until breakdown.

To confirm our model, we subject the same device as in Fig. 4 to a series of current stressing experiments under vacuum and expose it to air after a few stress cycles, as shown in Fig. 6.

Each data point in Fig. 6 is obtained after a three-minute stress cycle and after the device is cooled down to

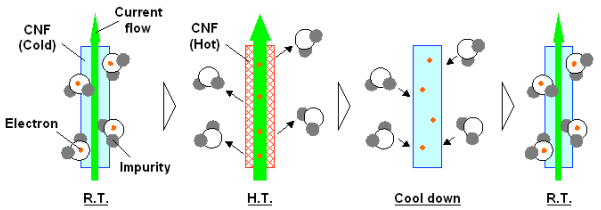

(a) Ambient

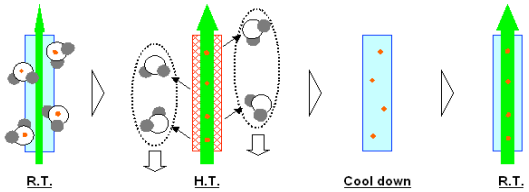

(b) Vacuum

Fig. 5 Model of molecular adsorption/desorption on CNF: (a) in ambient and (b) in vacuum.

room temperature. The stress current is increased in 100 μA steps up to 1000 μA and then exposed to air. This upper limit was chosen to avoid damage to the CNF, in order to isolate the suggested trapping/detrapping phenomenon. After stressing at 1000 μA, air is introduced into the chamber for 5 minutes, and the resistance is measured. This stress current cycle up to 1000 μA in 100 μA steps is then repeated, and the CNF is re-exposed to air for 10 minutes. Subsequently, the device is subjected to another series of stress cycles until breakdown at 2700 μA. The images shown in Fig. 4 are obtained during this final sequence of current stressing.

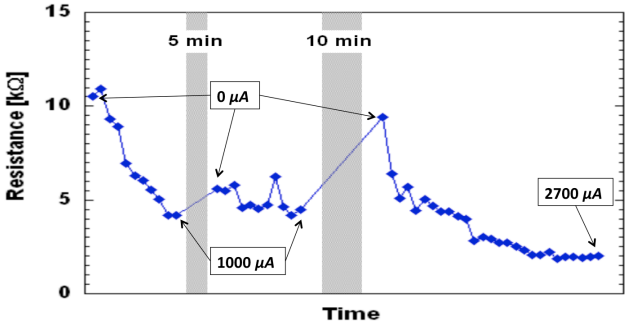

Fig. 6 Resistance of a CNF device in vacuum with intermittent exposure to air.

The resistance values in Fig. 6 show a decrease after successive stress current cycles, and an increase after exposure to air for each of the first two stages. Further, this resistance increase is higher when the air exposure time is longer. This behavior infers that the longer exposure time results in more molecules absorbed and consequently more carriers trapped, resulting in higher resistance. This result suggests that trapping by absorbed molecules is likely to dominate trapping due to defects in CNFs [12]. This finding is also consistent with the continuous resistance decrease with increasing stress current in the third stage (see Fig. 6). Such resistance decrease could not occur at such high stress currents if detrapping from defects were the dominant mechanism, since all carriers would have been de-trapped well before reaching these temperatures, preventing further decrease in resistance.

IV. ADSORPTION/DESORPTION MODEL

Assuming that trapped carriers by adsorbed molecules to be the principal underlying mechanism for our observed resistance behavior, we estimate the number of carriers detrapped during each stress cycle per cm^3, Δn, as follows.

$$\Delta\sigma = q\,(\Delta n)\mu \qquad (1)$$

$\Delta\sigma$ is the change in conductivity due to carrier detrapping, extracted from the difference in device resistance in ambient between heated (during current stressing) and cooled (after current stressing) states, q is the electron charge, and μ is the carrier mobility. The measured resistances after a stressing current of 400 μA is used for this estimation. We assume the mobility value for semiconducting CNTs (~100,000 $cm^2/V{\cdot}s$) [14] and scale it by the ratio of the conductivity of our CNF (2.6 x 10^2 S/cm), obtained by four-point probe measurement, to that of the reported CNTs (3.8 x 10^5 S/cm), such that $\mu_{CNF} = \mu_{CNT}$ ($\sigma_{CNF}/\sigma_{CNT}$) ~ 68 $cm^2/V{\cdot}s$. μ_{CNF} is assumed to be constant for this temperature variation and the difference in carrier density between CNF and CNT is neglected. For this CNF device, Δn is then estimated to be 4 x 10^{18} cm^{-3}, from the difference in resistance between heated and cooled states. From the CNF volume in this device, estimated to be 1.3 x 10^{-13} cm^3 from SEM images, the number of detrapped carriers ΔN due to Joule heating of this device at this stressing current is then 5 x 10^5. If we consider the CNF surface to be a graphene sheet, with atomic density 3.8 x 10^{15} cm^{-2}, the number of surface carbon atoms on this CNF N_C is 9.45 x 10^7, yielding a ratio $N_C/\Delta N$ ~ 190, or a density of adsorbed molecules of 2 x 10^{13} cm^{-2}. This areal density of adsorbed molecules is similar to results obtained from modeling semiconducting nanotubes exposed to a reducing gaseous species [17]. If we further assume that one carrier is released by one desorbed molecule, then this ratio infers that there is approximately one absorbed molecule present on this CNF per 190 surface carbon atoms.

While the result of this estimation does not definitively point to a specific adsorbed species, the fact that exposure to O_2 (electron acceptors) was reported to result in decreased resistance leads us to believe that oxygen in atmosphere is not likely to be the cause of our observed difference in resistance between room and high

temperatures. On the other hand, water vapor has also been reported to increase resistance in small concentrations for single-walled CNT mats. The same authors also found that degassing while heating their CNT mats resulted in decreasing the resistance. As CO_2 gas is also present in atmosphere and exposure to it was reported to increase the multi-walled CNT resistance, it is possible that CO_2 and/or water vapor in atmosphere are responsible for the observed resistance behavior of our CNF devices [15,16].

ACKNOWLEDGMENTS

The authors acknowledge the technical support from Hitachi High Technologies America. They are grateful to Philip D. Rack and David C. Joy of the University of Tennessee for their advice on electron-beam-induced tungsten depositions. This work was supported by the United States Army Space and Missile Defense Command (SMDC) and carries Distribution Statement A, approved for public release, distribution unlimited.

REFERENCES

[1] F. Kreupl, A. P. Graham, G. S. Duesberg, W. Steinhogl, M. Liebau, E. Unger, and W. Honlein, Microelectronic Engineering, **64**, 399 (2002).
[2] J. Li, Q. Ye, A. M. Cassell, H. T. Ng, R. Stevens, J. Han, and M. Meyyappan, Appl. Phys. Lett., **82**, 2491 (2003).
[3] M. Nihei, A. Kawabata, D. Kondo, M. Horibe, S. Sato, and Y. Awano, Jpn. J. Appl. Phys., Part 1 **44**, 1626 (2005).
[4] L. Zhang, D. Austin, V. I. Merkulov, A. V. Meleshko, K. L. Klein, M. A. Guillorn, D. H. Lowndes and M. L. Simpson, Appl. Phys. Lett., **84**, 3972 (2004).
[5] A. V. Melechko, V. I. Merkulov, T. E. McKnight, M. A. Guillorn, K. L. Klein, D. H. Lowndes, and M. L. Simpson, J. Appl. Phys., **97**, 041301 (2005).
[6] Q. Ngo, T. Yamada, M. Suzuki, Y. Ominami, A. M. Cassell, J. Li, M. Meyyappan, and C. Y. Yang, IEEE Trans. Nanotechnol., **6**, 688 (2007).
[7] H. Kitsuki, T. Yamada, D. Fabris, J. R. Jameson, P. Wilhite, M. Suzuki, and C. Y. Yang, Appl. Phys. Lett., **92**, 173110 (2008).
[8] T. Saito, T. Yamada, D. Fabris, H. Kitsuki, P. Wilhite, M. Suzuki, and C. Y. Yang, Appl. Phys. Lett., **93**, 102108 (2008).
[9] T. Yamada, T. Saito, D. Fabris, and C. Y. Yang, *IEEE Elec. Dev. Lett*., **30**, 469 (2009).
[10] B. A. Cruden, A. M. Cassell, Q. Ye, and M. Meyyappan, *J. Appl. Phys*., 94, 4070 (2003).
[11] P. D. Rack, J. D. Fowlkes, and S. J. Randolph, *Nanotechnology*, **18**, 465601 (2007).
[12] T. Yamada, H. Yabutani, T. Saito, and C. Y. Yang, *Nanotechnology*, **21**, 26707 (2010).
[13] P. G. Collins, M. Hersam, M. Arnold, R. Martel, and Ph. Avouris, *Phys. Rev. Lett.,* **86**, 3128 (2001).
[14] T. Dürkop, S. A. Getty, E. Cobas, and M. S. Fuhrer, *Nano Lett*., **4**, 35 (2004).
[15] A. Zahab, L. Spina, and P. Poncharal, *Phys. Rev. B*, **62**, 10000 (2001)
[16] K. G. Ong, K. Zeng, and C.A. Grime, *IEEE Sensors J.*, **2**, 2 (2002).
[17] T. Yamada, *Appl. Phys. Lett.,* **88**, 083106 (2006).